Solid-State ^{23}Na NMR Study of Sodium Lariat Ether Receptors Exhibiting Cation−π Interactions

David L. Bryce,*,† Samyuktha Adiga,† Elizabeth K. Elliott,‡ and George W. Gokel‡

Department of Chemistry and Centre for Catalysis Research and Innovation, University of Ottawa, Ottawa, Ontario K1N 6N5, Canada, and Departments of Molecular Biology and Pharmacology and Chemistry, Washington University School of Medicine, St. Louis, Missouri 63110

Received: August 10, 2006; In Final Form: October 5, 2006

Noncovalent cation−π interactions are important in a variety of supramolecular and biochemical systems. We present a ^{23}Na solid-state nuclear magnetic resonance (SSNMR) study of two sodium lariat ether complexes, **1** and **2**, in which a sodium cation interacts with an indolyl group that models the side chain of tryptophan. Sodium-23 SSNMR spectra of magic-angle spinning (MAS) and stationary powdered samples have been acquired at three magnetic field strengths (9.4, 11.75, 21.1 T) and analyzed to provide key information on the sodium electric field gradient and chemical shift (CS) tensors which are representative of the cation−π binding environment. Triple-quantum MAS NMR spectra acquired at 21.1 T clearly reveal two crystallographically distinct sites in both **1** and **2**. The quadrupolar coupling constants, $C_Q(^{23}Na)$, range from 2.92 ± 0.05 MHz for site A of **1** to 3.33 ± 0.05 MHz for site B of **2**; these values are somewhat larger than those reported previously by Wong et al. (Wong, A.; Whitehead, R. D.; Gan, Z.; Wu, G. *J. Phys. Chem. A* **2004**, *108*, 10551) for $NaBPh_4$, but very similar to the values obtained for sodium metallocenes by Willans and Schurko (Willans, M. J.; Schurko, R. W. *J. Phys. Chem. B* **2003**, *107*, 5144). We conclude from the 21.1 T data that the spans of the sodium CS tensors are less than 20 ppm for **1** and **2** and that the largest components of the EFG and CS tensors are non-coincident. Quantum chemical calculations of the NMR parameters substantiate the experimental findings and provide additional insight into the dependence of $C_Q(^{23}Na)$ on the proximity of the indole ring to Na^+. Taken together, this work has provided novel information on the NMR interaction tensors characteristic of a sodium cation interacting with a biologically important arene.

Introduction

Noncovalent interactions between a cation (e.g., alkali metal or ammonium cation) and a nearby π-system such as an aromatic ring,[1−3] alkene,[4,5] or alkyne[6] are known as cation−π interactions.[7−10] There is a large and growing body of experimental and theoretical data that has been collected with the goal of characterizing cation−π interactions and their impact on local molecular and electronic properties. These interactions have been posited to play important roles in diverse areas of chemistry including biomolecular recognition by proteins,[11−13] peptide stability,[14] protein−protein[15] and protein−DNA interactions,[16−19] ionophores and receptors,[20] nucleic acid structure and stability,[21,22] adsorption of small molecules in zeolites,[23−25] environmental systems,[26] and supramolecular recognition.[27−29] It has been shown experimentally, and reproduced theoretically,[30] that such interactions are relatively strong and may therefore be expected to have a significant impact on molecular and supramolecular structure. For example, the change in enthalpy, $-\Delta H^0$ (298 K), upon binding of an alkali metal cation to benzene in the gas phase is −76.6 kJ/mol for K^+,[7] −117.2 kJ/mol for Na^+,[8] and −158.7 kJ/mol for Li^+.[31] These values are well in excess of a typical hydrogen-bonding strength of ∼5 to 40 kJ/mol.

X-ray crystallographic studies of small molecules are valuable probes in the identification and characterization of cation−π interactions. To establish firm crystallographic evidence for cation−π interactions, one of us has designed and analyzed an extensive series of lariat ethers, wherein an alkali metal cation is complexed by a crown ether, and one or more side arms containing π-systems may interact with the cation.[1−6,32−37] One of the goals achieved in these studies has been the characterization of interactions that occur between alkali metal cations and neutral arenes of biological significance (e.g., indole groups). Unfortunately, crystallographic studies do not always provide conclusive details on the location or identity of bound ions in larger systems such as proteins. For example, Na^+ and H_2O, which both have 10 electrons, are not easily differentiated in the crystal structure of tryptophanase,[38] and it has been proposed[33] that electron density originally assigned to a water molecule may in fact be a sodium cation interacting with the aromatic ring of tyrosine 429. It is clear that complementary and/or alternative characterization methods are desirable.

Solid-state NMR (SSNMR) spectroscopy is an ideal tool for providing new physical insights[39,40] into the electronic structure about cations involved in cation−π interactions. Under favorable conditions, experiments performed on magic-angle spinning (MAS) and stationary powdered samples can yield information on the electric field gradient (EFG) tensor, the chemical shift (CS) tensor, and the relative orientations of these tensors.[41,42] In principle these two tensorial quantities offer different, complementary information on the bonding environment. Until recently, there has been little NMR spectroscopic characterization of cations involved in cation−π interactions,[43,44] particularly in the solid state. Recent work in this area has been nicely

* Author to whom correspondence should be addressed. Phone: 613-562-5800, ext 2018. Fax: 613-562-5170. E-mail: dbryce@uottawa.ca.
† University of Ottawa.
‡ Washington University School of Medicine.

10.1021/jp065171q CCC: $33.50
Published on Web 11/30/2006

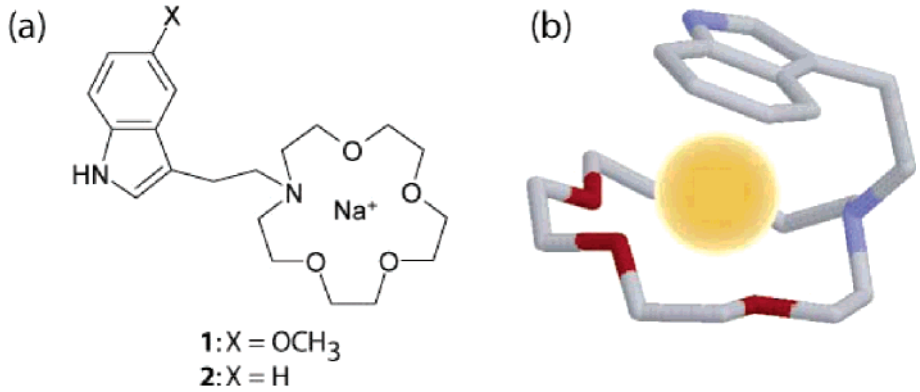

Figure 1. Structures of the sodium lariat ether salts studied in the present work. (a) Two-dimensional structural representation. (b) Three-dimensional representation of compound **2**; atomic coordinates were taken from refs 36 and 37; hydrogen atoms are not shown for clarity; the sodium cation is shown in orange. Both compounds crystallize with tetraphenylborate counterions (not shown).

summarized by Wong et al.[45] These same workers have also carried out a detailed ^{23}Na and ^{39}K SSNMR and computational study of sodium and potassium tetraphenylborates with the goal of establishing ^{23}Na and ^{39}K NMR signatures for alkali metal cations involved in cation−π bonding to phenyl rings.[45] Watts and co-workers[46,47] have discussed the important role of NMR spectroscopy in identifying cation−π interactions in the nicotinic acetylcholine receptor.[48]

Shown in Figure 1 are the structures of the two related sodium lariat ether complexes studied in the present work. These compounds are of particular interest in that they feature cation−π binding to an indolyl group, which is found in the side chain of tryptophan. As such, these complexes represent simple models for the interaction of sodium cations with tryptophan side chains in proteins. The goal of the present study is to apply ^{23}Na SSNMR spectroscopy to characterize this cation−π bonding environment to obtain new insights into the dependence of the observed NMR interaction tensors on the local molecular and electronic structure. Knowledge of the ^{23}Na EFG and CS tensors which are representative of cation−π binding to indole groups is an essential step in the interpretation of NMR data for larger systems for which alternative structural information is unavailable. Quantum chemical calculations are also employed to provide additional insights into the experimental data.

Experimental and Computational Methods

A. Sample Preparation. *Preparation of N-(2-(3-(5-methoxy)-indolyl)ethyl)aza-15-crown-5, Compound **1***: 5-Methoxytryptamine (0.53 g, 2.79 mmol), 1,14-bis(tosyloxy)-3,6,9,12-tetraoxatetradecane (1.53 g, 2.79 mmol), Na_2CO_3 (2.97 g, 28 mmol), NaI (20 mg, 0.13 mmol), and 40 mL of CH_3CN were combined and heated to reflux for 48 h. The solvent was removed in vacuo. The residue was dissolved in CH_2Cl_2, then washed with 2 × 50 mL each of 5% aq citric acid, 5% aq $NaHCO_3$, and brine solution. The organic layer was dried over $MgSO_4$, filtered through a Celite pad, and concentrated in vacuo. Column chromatography (0−5% Et_3N in Me_2CO) on silica resulted in a yellow oil (0.85 g, 93% yield). IR: 3220, 2875, 1485, 1456, 1353, 1217, 1117. ^{1}H NMR (300 MHz, CD_3COCD_3): δ 2.86−2.90 (m, 8H, $-CH_2CH_2N-$, $-NCH_{2-}$), 3.65−3.71 (m, 16H, $-CH_2OCH_{2-}$), 3.86 (s, 3H, $-OCH_3$), 6.85 (d, 1H, J = 2.4, indole-H7), 7.04 (dd, 2H, J = 2.4, J = 8.7, indole-H2,6), 7.24 (d, 1H, J = 8.7, indole-H4), 7.97 (s, 1H, indole-H1), 9.79 (s, 1H). ^{13}C NMR: 23.23, 54.72, 55.98, 57.45, 70.14, 70.19, 70.46, 71.07, 100.80, 111.73, 111.95, 114.22, 122.68, 128.01, 131.37, 153.89. Complex **1**·$NaBPh_4$: a 1:1 ratio of compound **1** and $NaBPH_4$ were dissolved in hot ethanol. Vapor diffusion of this solution with hexanes yielded colorless crystals (mp 154−156 °C).

The complex of $NaBPh_4$ with *N*-(2-(3-indolyl)ethyl)aza-15-crown-5, compound **2**, was prepared as described previously.[37] For the remainder of this manuscript, "**1**" and "**2**" refer to the $NaBPh_4$ complexes of these compounds.

B. Solid-State NMR Spectroscopy. Recrystallized samples of **1** and **2** were powdered and packed into the central tenth (lengthwise) of 4 mm o.d. zirconia MAS rotors. Only a few milligrams of **1** and **2** were used in these studies. Solid-state NMR spectra were recorded in magnetic fields of 9.4, 11.75, and 21.1 T (105.9, 132.3, and 238.1 MHz ^{23}Na Larmor frequency, respectively) using Bruker DSX, Avance, and Avance II consoles. Bruker XWinNMR (9.4 and 11.75 T) and TopSpin 1.3 (21.1 T) software was used for acquisition. At 9.4 and 21.1 T, Bruker double-resonance 4 mm MAS probes were used. At 11.75 T, a Bruker triple-resonance 4 mm MAS probe was used. MAS rates of 10−15 kHz were employed. Solid powdered NaCl or NaCl(aq) was used for pulse calibration. Typical central transition ("solid") $\pi/2$ pulses were 1.99, 2.36, and 1.55 μs at 9.4, 11.75, and 21.1 T, respectively. Shorter (e.g., $\pi/6$) pulses were used in some cases on stationary samples to ensure uniform excitation across the spectrum. Recycle delays ranged between 1 and 10 s. All 1D MAS spectra were obtained using a simple pulse−acquire sequence. Spectra of stationary powdered samples were acquired using a single-pulse or a spin−echo sequence ($\pi/2-\tau-\pi-\tau-$acquire). This sequence has been shown to provide optimal signal-to-noise with only a small signal distortion for half-integer spin quadrupolar nuclei.[49,50] High-power proton decoupling was employed during acquisition of the FID in all cases.

Two-dimensional rotor-synchronized ^{23}Na MQMAS spectra of compounds **1** and **2** were obtained at 21.1 T using a MAS rate of 11.111 kHz. The *z*-filtered 3QMAS pulse sequence[51] was used, consisting of excitation (6.6 μs) followed by evolution of the triple-quantum coherence during t_1 followed by a conversion pulse (2.2 μs), a 20 μs *z*-filter, and a selective $\pi/2$ pulse (13 μs) followed by acquisition during t_2. Radiofrequency fields were 81 kHz for the excitation and conversion pulses and 10 kHz for the third pulse. High-power proton decoupling was employed during t_1 and t_2. A recycle delay of 1.0 s was used. A total of 256 (compound **2**) or 512 (compound **1**) transients were obtained for each t_1 increment due to the small amount of sample available; 128 complex points were acquired in t_1, with a t_1 increment of 90 μs. Exponential apodization of 45 Hz was applied in both dimensions prior to zero-filling and Fourier transformation. The 2D spectra were sheared using TopSpin

1.3 to yield the isotropic dimension along F_1 and the anisotropic dimension along F_2. MQMAS spectra of compound **1** were also obtained at 11.75 T.

Experimentally, sodium-23 chemical shifts were measured with respect to the central transition centerband of NaCl(s). Reported sodium-23 chemical shift values, however, are with respect to $\delta(^{23}\text{Na})$ of dilute NaCl(aq). The CT centerband of solid NaCl is at +7.1 ppm on this scale.[52]

NMR spectra of stationary and MAS samples were simulated using WSOLIDS.[53] Stack plots were prepared using DMFit.[54]

C. Quantum Chemical Calculations. All quantum chemical calculations were performed using Gaussian 03.[55] A model for calculations of NMR interaction tensors was built using atomic coordinates for the heavy (non-hydrogen) atoms obtained from the X-ray crystal structure of compound **2** of Hu et al.[37] The model consisted of the sodium cation complexed by the lariat ether (see Figure 1b); the BPh_4^- counterion was not included in the model except where indicated. Hydrogen atoms were built on, and their positions were optimized at the B3LYP/6-311G* level while the positions of the heavy atoms remained fixed. Sodium electric field gradient and nuclear magnetic shielding (σ) tensors were subsequently calculated for the resulting optimized structure using the restricted Hartree−Fock (RHF) and B3LYP[56] methods with a series of Pople-type and Dunning-type basis sets. The gauge-including atomic orbitals (GIAO) method was used for the calculation of nuclear magnetic shielding tensors. Convergence-related options were left at their default values. The EFG and σ tensors were diagonalized (after symmetrization in the case of the shielding tensors) to yield three principal components and three Euler angles relating the orientation of their principal axis systems (PAS) to the local molecular coordinate system. The ^{23}Na quadrupolar coupling constant was obtained from the EFG tensor principal component of largest magnitude (V_{33}) according to the following equation:

$$C_Q = \frac{eV_{33}Q}{h} \quad (1)$$

where e is the charge on an electron, h is Planck's constant, and Q is the nuclear electric quadrupole moment for ^{23}Na, 10.4 fm^2 (ref 57). A factor of 9.7177×10^{21} V m^{-2} per atomic unit must also be included when using output directly from Gaussian 03. The asymmetry parameter of the EFG tensor is defined in terms of the principal components ($|V_{33}| \geq |V_{22}| \geq |V_{11}|$) as

$$\eta_Q = \frac{V_{11} - V_{22}}{V_{33}} \quad (2)$$

Additional models were constructed to provide physical insight into the dependence of the sodium NMR interaction tensors on the proximity of the indolyl aromatic system. To isolate this effect, no further geometry optimization was undertaken. Only the (indolyl-C3)−CH_2−CH_2−(aza-N) dihedral angle, ϕ, was systematically varied, from 30 to 180°, to produce new structural models which were then used for calculations of the EFG and nuclear magnetic shielding tensors.

Molecular orbital graphics were generated using GaussView 3.09.[58]

Results and Discussion

Solid-State NMR Spectroscopy. Sodium-23 ($I = {}^3/_2$; N.A. = 100%) is a quadrupolar nucleus with a high NMR receptivity (9.27×10^{-2} relative to ^{1}H) and a moderate nuclear electric quadrupole moment. Our general strategy for extracting the ^{23}Na quadrupolar coupling constant, asymmetry parameter, CS tensor, and the relative orientation of the EFG and CS tensors involves first acquiring NMR spectra under MAS conditions. Simulations of the resulting second-order quadrupolar line shape provide C_Q, η_Q, and δ_{iso}. With these parameters fixed, simulations of spectra acquired for stationary powdered samples will depend additionally on the magnitude of the CS tensor and its orientation relative to the EFG tensor.

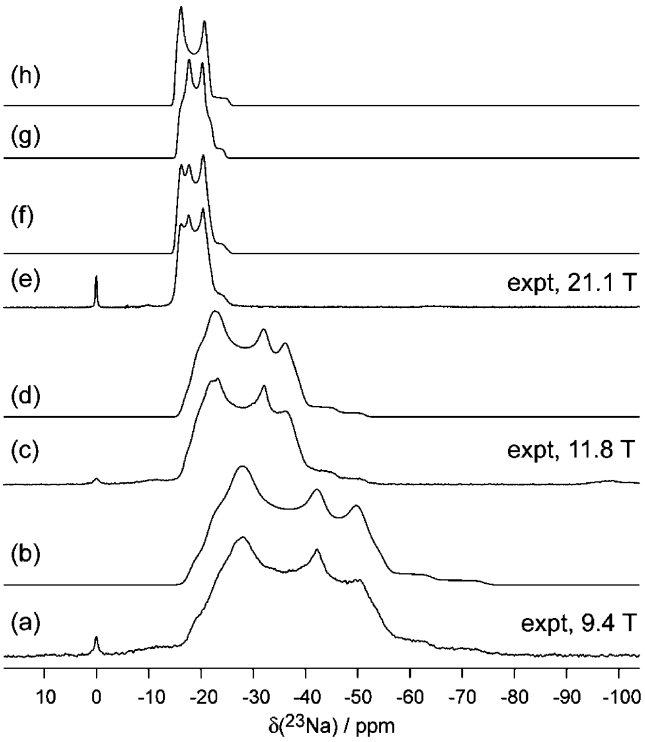

Figure 2. Solid-state ^{23}Na MAS NMR spectra of compound **1**. (a, c, e): Experimental ^{23}Na NMR spectra recorded with proton decoupling at MAS rates of 13 010, 10 000, and 11 111 Hz, respectively, in magnetic fields of 9.4, 11.8, and 21.1 T. A small peak due to a trace NaCl(s) impurity is evident at 0 ppm (experimentally, the spectra were referenced to NaCl(s) at 0 ppm). (b, d, f): Simulated spectra, each based on two crystallographically unique sodium sites, generated using the parameters given in Table 1. Also shown are the simulated line shapes (21.1 T) for each of the two unique sodium sites (site A shown in (g); site B shown in (h)).

Shown in Figure 2 are ^{23}Na NMR spectra obtained at 9.4, 11.8, and 21.1 T for MAS samples of compound **1**. The fact that high-quality spectra may be obtained under MAS conditions immediately indicates that the sodium nuclear quadrupolar coupling constants are not prohibitively large, which would result in very broad spectra, thereby complicating spectral acquisition and interpretation. Further inspection of the spectra in Figure 2 indicates that ideal second-order quadrupolar line shapes are present and that there appear to be two crystallographically and magnetically nonequivalent sodium sites in **1**. Spectral simulations confirm this through simultaneous fitting of spectra of MAS samples obtained at three magnetic field strengths. An alternative explanation is that there is a mixture of two polymorphs in our sample; however, this is unlikely given the high quality and small number of uniformly shaped crystals used to prepare the powdered NMR sample, and furthermore it is improbable that a mixture of two polymorphs would fortuitously exist in a 1:1 ratio. Presented in Table 1 are the values of $C_Q(^{23}\text{Na})$, η_Q, and δ_{iso} obtained. The values of $|C_Q|$, 2.92 ± 0.05 and 3.15 ± 0.08 MHz, for sites A and B, are significantly larger than those reported by Wong et al. for $NaBPh_4$, ($|C_Q| = 1.24 \pm 0.05$ MHz) wherein sodium cations

TABLE 1: Experimental Sodium-23 Quadrupolar and Chemical Shift Parameters Measured for Sodium Nuclei Involved in a Cation−π Interaction

compound	$C_Q(^{23}Na)$/MHz[a]	η_Q[b]	δ_{iso}/ppm[c]	Ω/ppm[d]	ref
1 (site A)	(+)2.92 ± 0.05	0.41 ± 0.04	−8.4 ± 1.5	7 ± 4	this work
1 (site B)	(+)3.15 ± 0.08	0.18 ± 0.04	−7.4 ± 1.5	4 ± 3	this work
2 (site A)	(+)3.10 ± 0.07	0.33 ± 0.04	−5.9 ± 1.5	<20	this work
2 (site B)	(+)3.33 ± 0.05	0.28 ± 0.04	−4.9 ± 1.5	<20	this work
Na[BPh$_4$]	(−)1.24 ± 0.05	0.0 ± 0.1	−45.6 ± 0.5	14 ± 2	Wong et al. (ref 45)

[a] Sign of C_Q inferred from quantum chemical calculations. [b] The quadrupolar asymmetry parameter, η_Q, is defined as $(V_{11} - V_{22})/V_{33}$, where $|V_{33}| \geq |V_{22}| \geq |V_{11}|$. [c] Chemical shifts are with respect to NaCl(aq). [d] The span, Ω, is defined as $\sigma_{33} - \sigma_{11} \approx \delta_{11} - \delta_{33}$, where $\sigma_{33} \geq \sigma_{22} \geq \sigma_{11}$ and $\delta_{11} \geq \delta_{22} \geq \delta_{33}$.

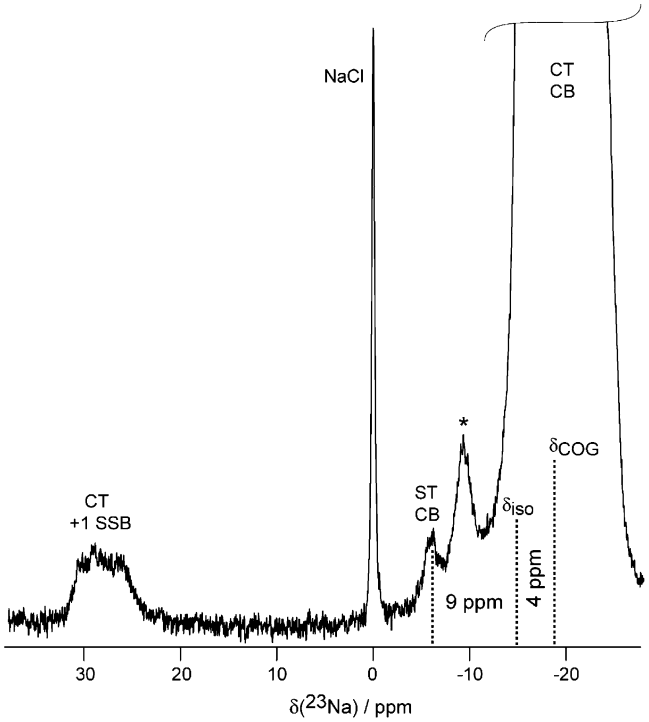

Figure 3. Expanded region of the ^{23}Na MAS NMR spectrum of **1** obtained at 21.1 T (MAS rate of 11 111 kHz). The central transition (CT) centerband (CB) is off scale at the low-frequency end of this expansion, and its center-of-gravity is marked at ~ −19 ppm as δ_{COG}. The true isotropic chemical shift (δ_{iso}) is 4 ppm to higher frequency. A further 9 ppm to higher frequency (~13 ppm from δ_{COG}) the satellite transition (ST, $\pm^3/_2$:$\pm^1/_2$) centerband is evident. Also shown are the central transition +1 spinning sideband (SSB), a trace NaCl(s) impurity at 0 ppm (experimentally, the spectra were referenced to NaCl(s) at 0 ppm), and a trace unknown impurity marked with an asterisk.

are interacting with the π-systems of the phenyl rings.[45] In the sodium and potassium tetraphenylborates, each cation is surrounded by four aromatic rings that, for symmetry reasons, may reduce the EFG at the cation.

Wong and Wu[59] have reported values of $C_Q(^{23}Na)$ for solid crown ethers, cryptands, and ionophores which range from 0.94 MHz for Na(*C*222)SCN to 3.15 MHz for Na(valinomycin)SCN; however, the values for crown ethers generally fall below 2 MHz. Importantly, the value obtained for sodium complexed in a crown ether of the same dimensions as those found in **1** and **2**, i.e., 15 atoms, is only 1.45 MHz (for Na(B15C5)I.H_2O), and the value reported for sodium complexed by 15-crown-5 itself is only 720 kHz,[60] suggesting that the presence of a cation−π interaction in **1** and **2** results in an increase in $C_Q(^{23}Na)$. Solution ^{23}Na NMR data also indicate relatively small quadrupolar coupling constants for sodium ions wrapped by crown ethers.[61,62] It is important to recognize that motional averaging in solution, or of symmetric complexes in the solid state, may reduce the effective EFG at sodium. Sodium-23 SSNMR data available for sodocenes[63] indicate that $C_Q(^{23}Na)$ values are very similar to those obtained for **1** and **2**, e.g., $C_Q(^{23}Na) = 3.07(2)$ MHz for Cp^{Me}Na.

TABLE 2: Second-Order ^{23}Na Quadrupolar Shifts for Sodium Lariat Ethers 1 and 2[a]

	11.75 T		21.1 T		
compound	$\delta_{iso} - \delta_{COG}$ (CT)/ppm	δ(ST) − δ_{COG}/ppm	$\delta_{iso} - \delta_{COG}$ (CT)/ppm	δ(ST) − δ_{COG}/ppm	observed δ(ST) − δ_{COG}/ppm
1 (site A)	12.9	38.6	4.0	12.0	13 ± 1
1 (site B)	14.3	43.0	4.4	13.3	13 ± 1
2 (site A)	14.2	42.7	4.4	13.3	
2 (site B)	16.3	48.8	5.0	15.1	

[a] See eqs 3 and 4. Data in the last column are observed experimentally. Results in the other columns are derived from data obtained from fitting the experimental central transition line shape.

The advantages of acquiring data at several field strengths were evident in the analysis of the MAS spectra. The data acquired at 21.1 T benefit from a marked reduction in the second-order quadrupolar broadening and a concomitant amplification of the isotropic chemical shift differences (in Hz) between the two sites in **1**. A detailed inspection of the spectrum obtained at 21.1 T (Figure 2e) is presented in Figure 3. It is well-known that the center-of-gravity (COG) of the central transition ($+^1/_2 \leftrightarrow -^1/_2$, CT) centerband (CB) is displaced from the true isotropic resonance frequency due to second-order quadrupolar effects.[64] For the present case of a spin $^3/_2$ nucleus, this displacement may be expressed in ppm as

$$\delta_{iso} - \delta_{COG} = \frac{1}{40}\left(\frac{C_Q^2}{\nu_L^2}\right)\left(1 + \frac{\eta_Q^2}{3}\right) \qquad (3)$$

where δ_{iso} is the true isotropic chemical shift, δ_{COG} is the apparent center-of-gravity shift of the CT centerband, and ν_L is the Larmor frequency of the nucleus under observation. The values of C_Q and η_Q obtained from the simulations of the CT line shape may be used to predict the displacement $\delta_{iso} - \delta_{COG}$; these are tabulated in Table 2 for $B_0 = 11.75$ and 21.1 T. The beneficial effects of the 21.1 T data are seen here, as the second-order shift is reduced from 12.9 to 4.0 ppm (site A) for **1**. As a further check on the quadrupolar parameters derived from line shape fitting, the position of the satellite transition ($\pm^3/_2 \leftrightarrow \pm^1/_2$, ST) centerband may be predicted and compared to what is observed in the experimental spectrum (Figure 3). For a spin $^3/_2$ nucleus, the ST centerband is shifted from the center-of-gravity of the CT by the following amount, in ppm:[64]

$$\delta(\mathrm{ST}) - \delta_{COG} = \frac{3}{40}\left(\frac{C_Q^2}{\nu_L^2}\right)\left(1 + \frac{\eta_Q^2}{3}\right) \qquad (4)$$

where δ(ST) is the shift of the satellite transition centerband. Values of δ(ST) − δ_{COG} predicted on the basis of CT line shape

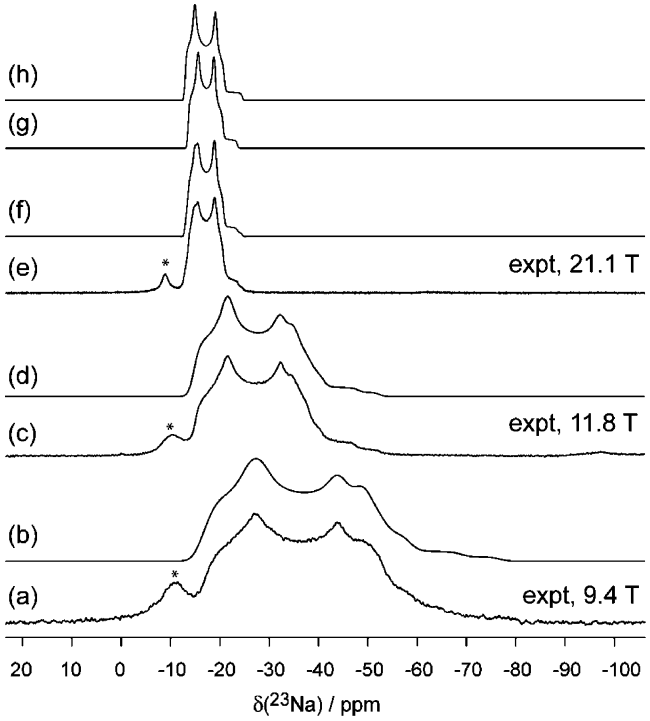

Figure 4. Solid-state ^{23}Na MAS NMR spectra of compound **2**. (a, c, e): Experimental ^{23}Na NMR spectra recorded with proton decoupling at MAS rates of 10 000, 10 000, and 11 111 Hz, respectively, in magnetic fields of 9.4, 11.8, and 21.1 T. A peak due to an unknown impurity is indicated with an asterisk. (b, d, f): Simulated spectra, each based on two crystallographically unique sodium sites, generated using the parameters given in Table 1. Also shown are the simulated line shapes (21.1 T) for each of the two unique sodium sites (site A shown in (g); site B shown in (h)). Experimentally, the spectra were referenced to NaCl(s) at 0 ppm.

fitting are summarized in Table 2. In the case of compound **1**, the ST centerband is observed in the spectrum (Figure 3) at 13 ppm with respect to δ_{COG} and at 9 ppm with respect to the value of δ_{iso}. These observations are in excellent agreement with the values predicted on the basis of the parameters obtained from line shape fitting (Table 2).

Sodium-23 NMR spectra of MAS samples of compound **2** are presented in Figure 4. Again, data were acquired at three magnetic field strengths, and this proved to be very beneficial for spectral simulations. Two nonequivalent sodium sites are once again observed, as was the case for **1**. The values of $C_Q(^{23}Na)$, η_Q, and δ_{iso} obtained from line shape fitting are presented in Table 1. The parameters are very similar to those obtained for **1**; this is not surprising as the two compounds differ only in a substituent on the indole ring (see Figure 1). The values of $|C_Q|$, 3.10 $\pm$ 0.07 and 3.33 $\pm$ 0.05 MHz, are 6% larger than the values obtained for the two nonequivalent sites in **1**. The successful analysis of the spectra presented in Figure 4 again speaks to the fact that ^{23}Na solid-state NMR spectroscopy offers resolution of sodium sites in very similar, but not identical, cation$-\pi$ binding environments. Second-order quadrupolar shifts and satellite transition shifts for **2** are presented in Table 2; however, the presence of a small impurity precluded the experimental observation of the ST centerband in this case. Interestingly, X-ray crystal structure data available for **2** indicate only a single sodium site in the asymmetric unit;[36] however, the NMR data clearly indicate two equally populated sites. A preliminary report[65] stated that the unit cell indeed contains two crystallographically distinct sodium sites, in agreement with the NMR results.

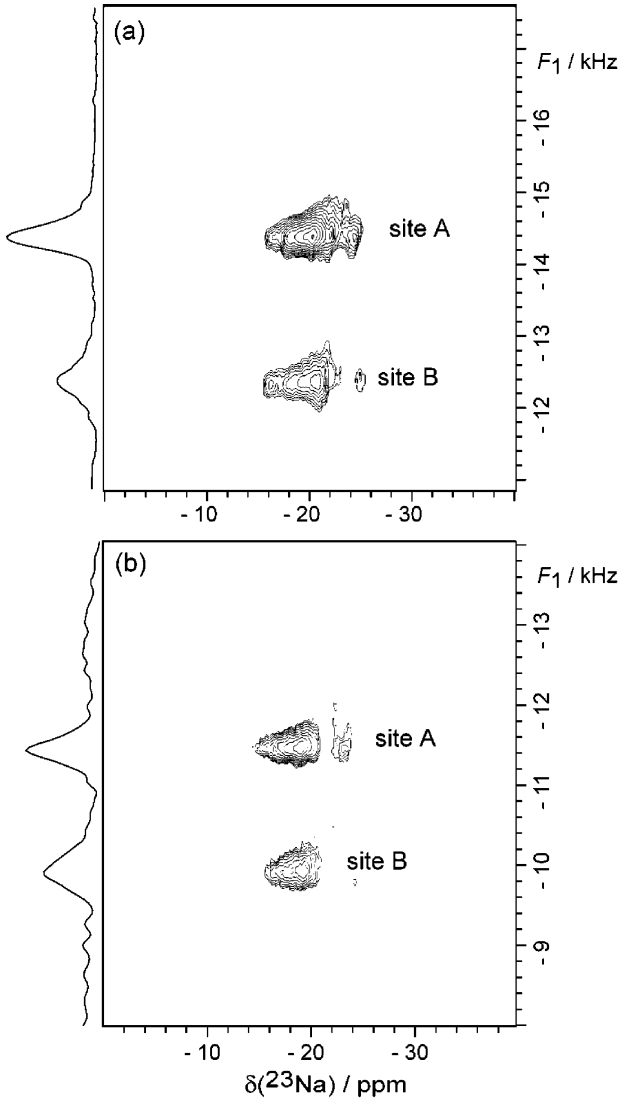

Figure 5. ^{23}Na MQMAS NMR spectra obtained at 21.1 T for (a) compound **1**; (b) compound **2**.

Sodium-23 MQMAS[51,66−68] NMR spectra were recorded at 21.1 T for **1** and **2** (Figure 5) as further evidence for the existence of two nonequivalent sodium sites in each of these compounds, and to provide additional experimental restraints for the one-dimensional line shape simulations. For potential future analyses of alkali metal cations involved in cation$-\pi$ interactions in larger biomolecular systems, the present results are encouraging in that spectral resolution is obtained for two very similar sodium environments. Resolution of sodium sites by MQMAS has also been demonstrated recently by Grant et al. for sodium mononucleotide complexes in which sodium cations are coordinated by phosphate and water oxygen atoms.[69] This could be important in larger biomolecular systems where several sodium cations may be bound to similar sites of interest in a given sample.

Having firmly established the quadrupolar parameters for **1** and **2** through one- and two-dimensional MAS NMR, spectra of stationary samples were recorded with the goal of extracting the sodium CS tensor magnitude and its orientation relative to the EFG tensor. Such data are important since the two tensors report on different aspects of the local and longer-range molecular and electronic structure about the sodium cation. Furthermore, as very high magnetic fields, e.g., 18.8 or 21.1 T or beyond, become more commonplace, proper spectral inter-

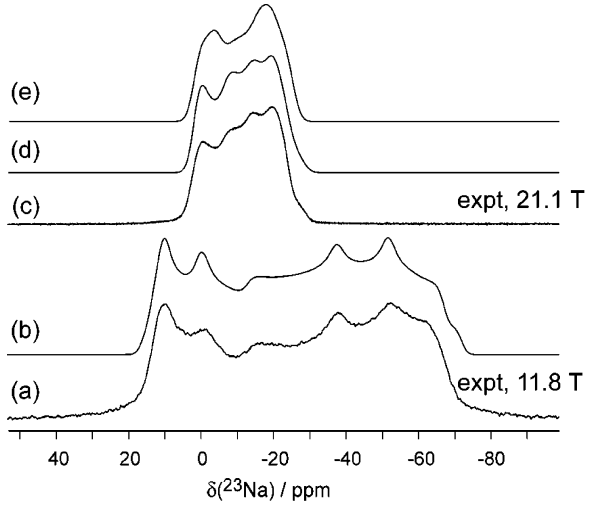

Figure 6. Solid-state ^{23}Na spectra of stationary powdered samples of compound **1**. (a, c): Experimental ^{23}Na NMR spectra recorded with proton decoupling in magnetic fields of 11.8 and 21.1 T. (b, d): Simulated spectra, each based on two crystallographically unique sodium sites, generated using the quadrupolar parameters given in Table 1 and the CS tensor parameters reported in the text. Shown in (e) is the spectral simulation (21.1 T) resulting if anisotropy of the chemical shift tensor for both sites is set to zero in the simulation. Experimentally, the spectra were referenced to NaCl(s) at 0 ppm.

pretation for quadrupolar nuclei must include the effects of chemical shift anisotropy.

Presented in Figure 6 are ^{23}Na NMR spectra of stationary samples of **1** obtained at 11.8 and 21.1 T. Spectral simulations specify that the span,[70] $\Omega = \delta_{11} - \delta_{33}$, of the sodium CS tensor is 7 ± 4 ppm for site A and 4 ± 3 ppm for site B. Other parameters used in these simulations include the skew of the CS tensor, $\kappa = 3(\delta_{22} - \delta_{iso})/\Omega$, which was set to 0.4 ± 0.4 for site A and to 0.7 ± 0.3 for site B, and the Euler angles describing the rotations required to bring the PAS of the EFG tensor into coincidence with that of the CS tensor.[71] These angles are $\alpha = 86° \pm 20°$, $\beta = 84° \pm 20°$, $\gamma = 90° \pm 20°$ for site A and $\alpha = 0° \pm 20°$, $\beta = 78° \pm 30°$, $\gamma = 33° \pm 40°$ for site B. It is evident that a more precise characterization of these angles is not realistic given the very small anisotropy of the CS tensor. It is also important to not rule out the fact that alternate sets of Euler angles may also fit the experimental data; however, repeated simulations indicate clearly that the angle β must be significantly different from zero, which means that the largest components of the magnetic shielding and EFG tensors are not coincident. It is also clear that the data cannot be fit in the absence of a span on the order of 5 ppm for both sites.

Although these are very small spans, it is apparent that the anisotropy of the CS tensor has an important effect on the observed line shape. For example, shown in Figure 6e is the ^{23}Na spectrum expected if the sodium CS tensor were completely isotropic. The CS tensor spans are smaller than, but comparable to, those obtained by Willans and Schurko[63] for sodium metallocenes ($\Omega = 9.5-12.5$ ppm) as well as those obtained by Wu and co-workers for $NaBPh_4$ ($\Omega = 14 \pm 2$ ppm)[45] and Na(12-crown-4)$_2$ClO$_4$ ($\Omega = 14$ ppm).[59] The sodium CS tensor spans are similarly small in a series of inorganic salts studied using single-crystal NMR by Sagnowski et al., $\Omega(NaNO_3) = 0 \pm 2$ ppm; $\Omega(NaClO_3) = 12 \pm 2$ ppm; $\Omega(NaBrO_3) = 17 \pm 2$ ppm.[72] The present conclusion that the largest components of the magnetic shielding and EFG tensors are not coincident, e.g., in fact σ_{11} and V_{33} are coincident for site B, is in contrast to the situation observed for $NaBPh_4$ and the sodocenes.

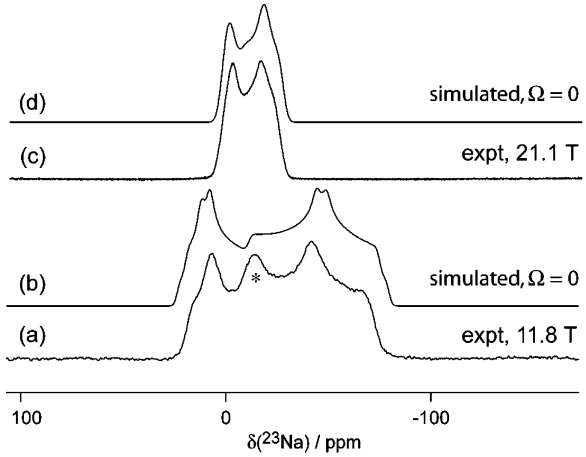

Figure 7. Solid-state ^{23}Na spectra of stationary powdered samples of compound **2**. (a, c): Experimental ^{23}Na NMR spectra recorded with proton decoupling in magnetic fields of 11.8 and 21.1 T. (b, d): Simulated spectra, each based on two crystallographically unique sodium sites, generated using the quadrupolar parameters given in Table 1 and assuming an isotropic chemical shift tensor ($\Omega = 0$). Experimentally, the spectra were referenced to NaCl(s) at 0 ppm.

Shown in Figure 7 are the experimental ^{23}Na NMR spectra of stationary samples of **2**. Unfortunately, a small impurity in this sample (denoted by asterisks in Figures 4 and 7) precludes an accurate determination of the CS tensor parameters; nevertheless, simulations show that it is clear that the span is of the same order of magnitude as that found in compound **1**. An upper limit of 20 ppm is reported in Table 1; this is in accord with a calculated span of 14.4 ppm for Na^+ interacting with the five-membered ring of tryptophan.[45] Simulated spectra which assume an isotropic CS tensor are presented in Figure 7 along with the experimental spectra, and it is clear that a small but non-negligible contribution from the sodium CSA exists. The fact that the experimental spectra are *narrower* than the simulated zero-span spectra suggests that the observed differences between experimental and simulated spectra are not due to dipolar couplings (e.g., ^{23}Na−^{23}Na) and also suggests that σ_{33} and V_{33} are non-coincident as is the case for compound **1**.

The small sodium CS tensor spans observed experimentally strongly suggest the lack of significant contributions to the paramagnetic part of the nuclear magnetic shielding tensor. This is discussed below in the context of quantum chemical calculations (vide infra).

Quantum Chemical Calculations and Interpretation of NMR Parameters. A series of quantum chemical calculations of the sodium nuclear magnetic shielding and EFG tensors was carried out on compound **2** to provide added insight into the experimental results. The results of the calculations, carried out at the RHF and B3LYP levels, are tabulated in Table 3. The experimental values of $C_Q(^{23}Na)$ are best reproduced by the Dunning-type cc-pVXZ (X = D,T) basis sets,[73,74] using either the RHF or B3LYP method. For example, an RHF/cc-pVTZ calculation of the EFG tensor results in a C_Q of 3.10 MHz, whereas the experimental value for site A of compound **2** is 3.10 ± 0.07 MHz. The calculations also indicate that the sign of the quadrupolar coupling constant is positive. Interestingly, this is in contrast to the negative values of C_Q reported for $NaBPh_4$, in which Na^+ is also involved in a cation−π interaction.[45] Calculated values of η_Q are generally not within experimental error; however, for the larger basis sets they are consistently less than 0.4, in agreement with experiment. Of the data reported in Table 3, only the small 3-21G basis set not surprisingly yields equivocal results. The modest 6-31G basis

TABLE 3: Quantum Chemical Calculations of the Sodium-23 Quadrupolar and Nuclear Magnetic Shielding Tensors for Lariat Ether 2[a]

method and basis set	C_Q/MHz	η_Q	σ_{11}/ppm	σ_{22}/ppm	σ_{33}/ppm	σ_{iso}/ppm	δ_{iso}/ppm[b]	Ω/ppm
RHF/3-21G	−1.09	0.76	596.2	600.7	607.9	601.6	−25.0	11.7
RHF/6-31G	3.10	0.21	586.8	591.1	595.7	591.2	−14.6	8.9
RHF/6-311G*	4.33	0.19	576.7	581.4	588.0	582.0	−5.4	11.3
RHF/6-311++G**	4.34	0.20	576.8	581.7	588.2	582.2	−5.6	11.4
RHF/cc-pVDZ	2.93	0.10	586.3	594.1	598.9	593.1	−16.5	12.6
RHF/cc-pVTZ	3.10	0.14	584.5	589.2	595.7	589.8	−13.2	11.2
B3LYP/3-21G	−1.20	0.85	568.2	591.8	598.7	586.2	−9.6	30.5
B3LYP/6-31G	3.04	0.16	575.7	579.9	584.1	579.9	−3.3	8.4
B3LYP/6-311G	4.60	0.22	565.5	570.3	575.6	570.5	6.1	10.1
B3LYP/6-311G*	4.41	0.18	564.6	569.2	574.6	569.5	7.1	10.0
B3LYP/6-311++G	4.59	0.22	564.9	570.7	575.6	570.4	6.2	10.7
B3LYP/6-311++G**	4.42	0.19	564.9	570.0	575.1	570.0	6.6	10.2
B3LYP/cc-pVDZ	3.02	0.11	576.3	586.7	593.2	585.4	−8.8	16.9
B3LYP/cc-pVTZ	3.05	0.10	572.0	578.2	582.6	577.6	−1.0	10.6

[a] Proton positions were optimized at the B3LYP/6-311G* level. [b] Values are reported with respect to NaCl(aq) at 0 ppm. Calculated values of σ_{iso} were converted to δ_{iso} by using the following relation: δ_{iso}(wrt NaCl(aq)) = 576.6 ppm − σ_{iso}

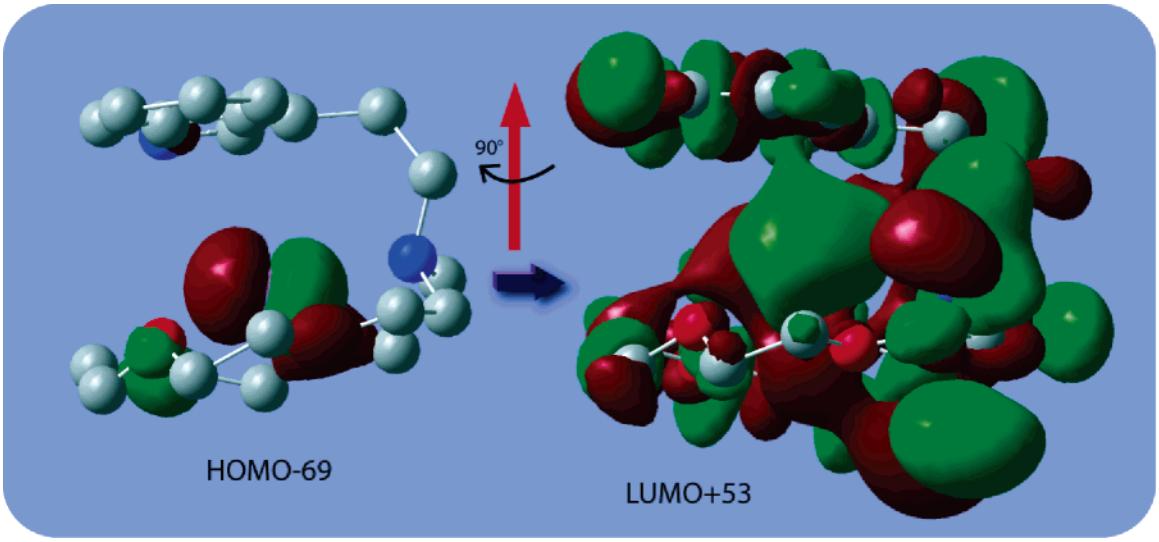

Figure 8. Selected pair of occupied (HOMO−69) and virtual (LUMO+53) orbitals which contribute to paramagnetic deshielding along the σ_{11} direction (i.e., approximately perpendicular to the plane of the indole ring, as depicted by the red arrow). The relevant orbital overlap may be visualized by rotating the p-type orbital (HOMO−69) on sodium 90° about the red arrow, while keeping the atomic coordinates fixed. The resulting rotated p-type orbital overlaps favorably at sodium with the LUMO+53 orbital. Hydrogen atoms are not shown for clarity. Figure generated using GaussView 3.09 (ref 58).

set, used within either the RHF or B3LYP framework, yields values of C_Q which are within experimental error.

Small discrepancies between experimental and theoretical values obtained here may originate from the fact that calculations are carried out on an isolated cationic system in vacuo, whereas the experiments have been carried out in the solid state, with a surrounding lattice of neighboring cations and anions. The effect of including the nearest neighbor tetraphenylborate counterion on the computed NMR parameters of **2** was investigated. While the effect on the calculated nuclear magnetic shielding tensor spans is negligible, the value of C_Q changes from 3.10 to 3.25 MHz at the RHF/6-31G level and from 3.04 to 3.46 MHz at the B3LYP/6-31G level when the counterion is added (see the Supporting Information for further details). These results demonstrate that the surrounding crystal lattice can have an important effect on the EFG tensor at sodium; however, caution must be exercised when building an appropriate model of this lattice. In the present case only a single counterion could be included, and a somewhat asymmetric model of the effects of the lattice results. For this reason, the isolated cation model seems to provide results of approximately equal reliability in the present case. A plane-wave-based description of the system, such as that as described by Pickard and Mauri,[75] is a useful method to incorporate crystal lattice effects during the calculation of NMR parameters.

Calculations of the sodium nuclear magnetic shielding tensor in isolated cationic **2** (Table 3) reproduce the experimental finding that $\Omega < 20$ ppm. For example, the B3LYP/cc-pVTZ result is $\Omega = 10.6$ ppm. The largest component of the EFG tensor, V_{33}, is oriented approximately perpendicular to the average plane of the crown ether and passes through the indolyl C_{7a} carbon atom (see the Supporting Information). It is satisfying to note that the *least* shielded component of the shielding tensor is approximately coincident (within 6° at this level of theory) with V_{33}; this is in agreement with the relative tensor orientations derived experimentally for compound **1**, vide supra. The small values of Ω may be rationalized in the context of Ramsey's theory,[76−80] which describes how the paramagnetic contribution to the shielding tensor (σ_p) is related to magnetic-dipole-allowed mixing of occupied and virtual orbitals. The degree to which the mixing results in a deshielding of one of the principal components of the shielding tensor depends on the degree of occupied/virtual orbital overlap after application of an orbital angular momentum operator and on the inverse of the energy gap separating these orbitals. Consistent with experiment, an analysis of the molecular orbitals (MO) obtained from a B3LYP/

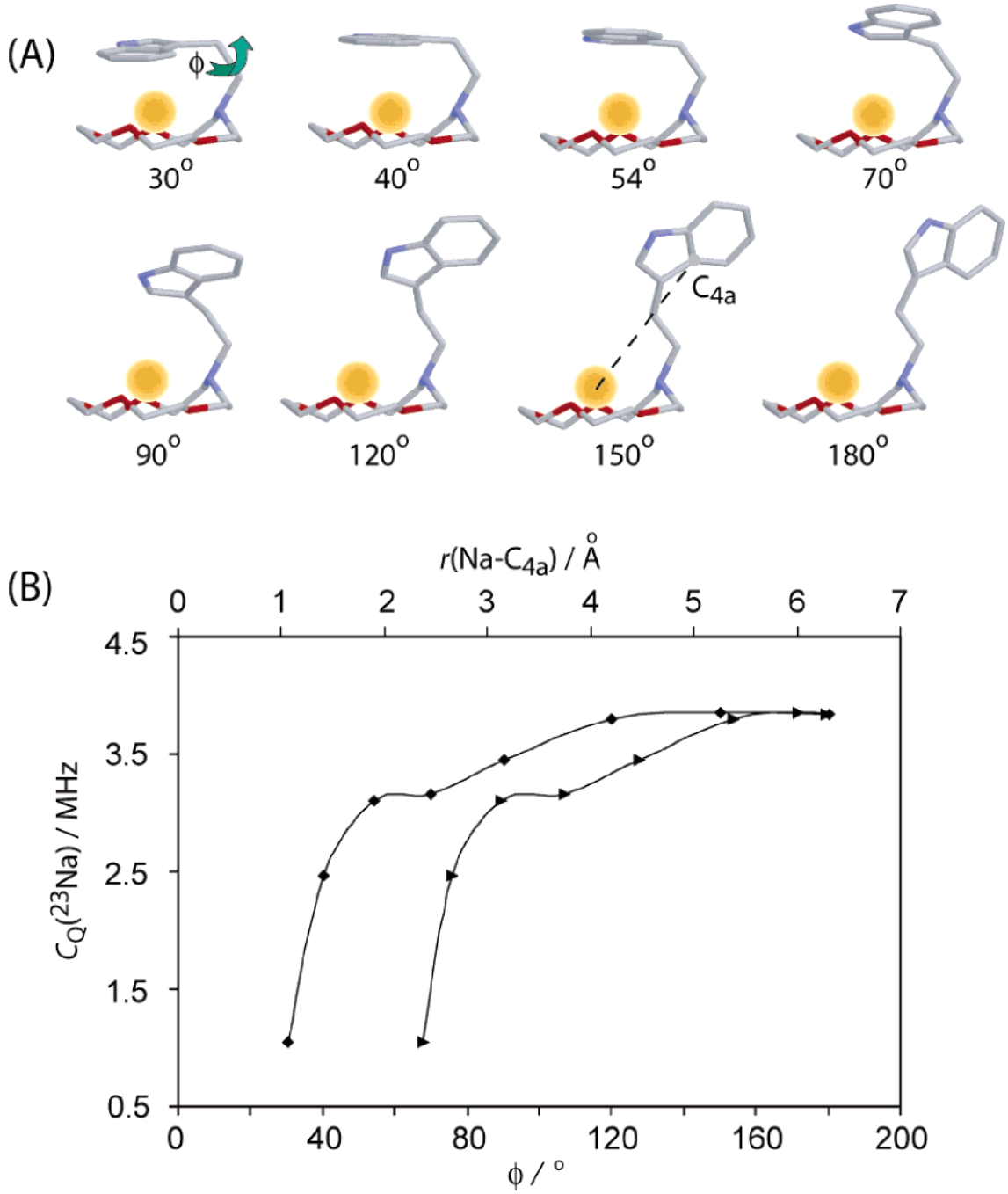

Figure 9. (A) Geometries used to investigate the effect of the proximity of the indolyl moiety on the NMR parameters of the sodium cation in compound **2**. Hydrogen atoms are omitted for clarity. Each structure differs from the next only in that a rotation about the (indolyl-C3)−CH_2−CH_2–(aza-N) dihedral angle, ϕ, has been made (see green arrow). In the experimental structure, this dihedral angle is ~54°. (B) Sodium-23 quadrupolar coupling constants as a function of ϕ (diamonds, lower axis) and of the Na−C_{4a} distance (triangles, upper axis); RHF/cc-pVTZ results.

6-31G calculation on **2** reveals that appropriate occupied orbitals for contributions to σ_p, i.e., those which feature large sodium p-type orbital contributions, lie significantly below the HOMO−LUMO gap (e.g., HOMO−69, see Figure 8). The energy gap between HOMO−69 and a virtual orbital featuring contributions of appropriate symmetry on sodium, e.g., LUMO+53, is 113 kJ/mol. The mixing of this pair of MOs also qualitatively explains why the least shielded component, σ_{11}, is oriented perpendicular to the plane of the aromatic ring (see Figure 8). Nevertheless, it is clear that the deshielding contribution to σ_{11} is a very small and subtle effect, as evidenced by the very small spans obtained experimentally and theoretically.

The absolute shielding scale[81] for ^{23}Na, derived from atomic beam magnetic resonance and relativistic calculations,[82] makes use of the ^{23}Na magnetic shielding constant for infinitely dilute Na^+ ions in D_2O at 297 K and allows for comparison between experimentally measured chemical shifts and calculated magnetic shielding constants:

$$\delta_{iso} = \frac{576.6\text{ppm} - \sigma_{iso}}{1 - 576.6\text{ppm}} \approx 576.6\text{ppm} - \sigma_{iso} \qquad (5)$$

The derived chemical shifts, presented in Table 3, are interesting to compare with experiment. The RHF/6-311G* and RHF/6-311++G** results, −5.4 and −5.6 ppm, respectively, are well within experimental error of the observed values for site A and B, −5.9 ± 1.5 ppm and −4.9 ± 1.5 ppm. RHF calculations with the cc-pVDZ and cc-pVTZ basis sets produce chemical

TABLE 4: Computed (RHF/cc-pVTZ) Variation of Sodium-23 Quadrupolar and Nuclear Magnetic Shielding Tensors as a Function of (Indolyl-C3)−CH_2−CH_2−(aza-N) Dihedral Angle, ϕ, in Lariat Ether Compound 2[a]

angle/(deg)	C_Q/MHz	η_Q	σ_{11}/ppm	σ_{22}/ppm	σ_{33}/ppm	σ_{iso}/ppm	δ_{iso}/ppm[b]
30	1.05	0.26	563.8	574.8	591.3	576.6	0.0
40	2.46	0.15	580.6	588.2	591.9	586.9	−10.3
54	3.10	0.14	584.5	589.2	595.7	589.8	−13.2
70	3.15	0.15	580.6	585.6	592.5	586.2	−9.6
90	3.45	0.14	578.3	584.7	592.2	585.1	−8.5
120	3.80	0.12	576.1	587.5	594.0	585.9	−9.3
150	3.84	0.13	575.5	588.2	594.4	586.0	−9.4
180	3.84	0.13	575.5	588.3	594.6	586.1	−9.5

[a] See the Supporting Information for additional data (results at different levels of theory). [b] See the footnote *b* of Table 3.

shifts, −16.5 and −13.2 ppm, which are ∼10 ppm too shielded relative to experiment, whereas B3LYP calculations with these basis sets provide results that are within a few ppm of experiment.

While the use of an absolute shielding scale enables the most stringent test of the ability of a theory to reproduce magnetic shielding constants, the use of quantum chemically calculated shielding constants of reference compounds to derive chemical shifts (i.e., differences between shielding constants) is also worth exploring. Wong et al. have reported calculated isotropic shielding constants at various levels of theory for $[Na(H_2O)_6]^+$, which is representative of aqueous NaCl. Their calculated values range from 571.8 ppm at the B3LYP/6-311G(d,p) level to 588.7 ppm at the HF/6-31G(d)/cc-pVDZ level. Use of this latter value as a shielding reference results in improved agreement with experiment for the RHF/cc-pVDZ and RHF/cc-pVTZ calculations, −4.4 and −1.1 ppm. However, this improvement is somewhat fortuitous given that the shielding constant for the reference was derived at a different level of theory.

To develop additional insight into the dependence of the sodium NMR interaction tensors on the proximity of the π-system contained within the indolyl moiety, a series of calculations was performed wherein the (indolyl-C3)−CH_2−CH_2−(aza-N) dihedral angle, ϕ, was systematically varied to produce a set of model structures (Figure 9A). This dihedral angle is approximately 54° in the X-ray structure of **2**. Variations in the NMR parameters as a function of the proximity of the π-system may be useful in the interpretation of ^{23}Na data in systems where alternative structural information is unavailable. The observed trend in $C_Q(^{23}Na)$ is depicted in Figure 9B, both as a function of ϕ and as a function of the distance from Na^+ to the fusion carbon C_{4a}. The value of C_Q increases sharply as a function of ϕ for values of ϕ between ∼30° and ∼90°. This is very interesting as, in the present system, it is this range of values that represent physically realistic situations for which a cation−π interaction may be supposed. For larger values of ϕ, the indolyl moiety is far removed from the sodium cation (Figure 9), and the value of C_Q plateaus. The calculations, in concert with the experimental quadrupolar coupling constants, suggest that the indolyl group is slightly closer to the sodium cation in compound **1** than in compound **2**.

Interestingly, as shown in Table 4, the experimental structure (ϕ = 54°) produces the most shielded chemical shift, in agreement with the conclusions of Wong et al. that highly shielded resonances are characteristic of cation−π interactions.[45] However, it is important to note that the chemical shifts observed experimentally for **1** and **2**, while somewhat shielded, are ∼40 ppm less shielded than those observed for $NaBPh_4$.

Conclusion

Cation−π interactions in two sodium lariat ether complexes have been characterized by solid-state ^{23}Na NMR spectroscopy and quantum chemistry. In addition to providing benchmark ^{23}Na quadrupolar coupling constants for sodium interacting with the tryptophan side chain, useful information on the sodium chemical shift tensors has been gleaned. As such, this study has provided new information on the NMR interaction tensors characteristic of a sodium cation interacting with a biologically significant arene. This new information is complementary to other recent experimental and theoretical work which has specifically examined interactions involving tryptophan.[83,84]

Particularly shielded isotropic chemical shifts seem to be associated with the presence of the cation−π interaction; however, it is difficult to conclusively associate a single isotropic observable with the presence or absence of a cation−π interaction. Taken together, the EFG and CS tensor data presented herein are characteristic of the sodium−indolyl bonding environment. Quantum chemical calculations of the sodium EFG and nuclear magnetic shielding tensors corroborate the experimental data, including the new insight that the largest components of these tensors are non-coincident.

The use of a 21.1 T NMR spectrometer offered three crucial advantages in the present study. First, the increased signal-to-noise and concomitant time savings that this high field strength affords was particularly beneficial since only a few milligrams of sample were available. Second, the increased chemical shift resolution at this high field enabled accurate spectral simulations, in particular the definitive resolution of two crystallographically nonequivalent sodium sites. This is an important consideration if solid-state NMR is to be applied to study quadrupolar nuclei such as ^{23}Na and ^{39}K in larger biomolecular systems for which significant spectral overlap from several similar binding sites is possible. Finally, the measurement of ^{23}Na CS tensor spans on the order of 5 ppm would not have been possible at lower fields in this case where two very similar powder patterns due to the different sites completely overlap.

Acknowledgment. We are grateful to Victor Terskikh and Glenn Facey for technical assistance and helpful discussions. We thank Igor Moudrakovski for access to the Steacie Institute for Molecular Sciences (NRC, Ottawa) 400 MHz spectrometer. We also thank Martine Monette, Stefan Steuernagel, Gang Wu, and Scott Kroeker for helpful advice concerning MQMAS experiments. Access to the 900 MHz NMR spectrometer was provided by the National Ultrahigh-Field NMR Facility for Solids (Ottawa, Canada), a national research facility funded by the Canada Foundation for Innovation, the Ontario Innovation Trust, Recherche Québec, the National Research Council of Canada, and Bruker Biospin and managed by the University of Ottawa (www.nmr900.ca). Some calculations were carried out using the High-Performance Virtual Computing Laboratory (HPCVL). D.L.B. thanks the Natural Sciences and Engineering Research Council (NSERC) of Canada for generous funding, and S.A. thanks NSERC for an Undergraduate Student Research Award. G.W.G. and E.K.E. thank the U.S. National Science Foundation for support.

Supporting Information Available: One figure showing the calculated tensor orientations, one table summarizing the effect of the counterion on the calculated NMR parameters, and one table containing calculated parameters as a function of ϕ for various levels of theory. This material is available free of charge via the Internet at http://pubs.acs.org.

References and Notes

(1) Gokel, G. W. *Chem. Commun.* **2003**, 2847.

(2) De Wall, S. L.; Barbour, L. J.; Gokel, G. W. *J. Am. Chem. Soc.* **1999**, *121*, 8405.

(3) De Wall, S. L.; Meadows, E. S.; Barbour, L. J.; Gokel, G. W. *J. Am. Chem. Soc.* **1999**, *121*, 5613.

(4) Hu, J.; Barbour, L. J.; Gokel, G. W. *Chem. Commun.* **2001**, 1858.

(5) Hu, J.; Barbour, L. J.; Gokel, G. W. *Collect. Czech. Chem. Commun.* **2004**, *69*, 1050.

(6) Hu, J.; Barbour, L. J.; Gokel, G. W. *J. Am. Chem. Soc.* **2001**, *123*, 9486.

(7) Sunner, J.; Nishizawa, K.; Kebarle, P. *J. Phys. Chem.* **1981**, *85*, 1814.

(8) Guo, B. C.; Purnell, J. W.; Castleman, A. W., Jr. *Chem. Phys. Lett.* **1990**, *168*, 155.

(9) Ma, J. C.; Dougherty, D. A. *Chem. Rev.* **1997**, *97*, 1303.

(10) Gokel, G. W.; De Wall, S. L.; Meadows, E. S. *Eur. J. Org. Chem.* **2000**, 2967.

(11) Scrutton, N. S.; Raine, A. R. C. *Biochem. J.* **1996**, *319*, 1.

(12) Dougherty, D. A. *Science* **1996**, *271*, 163.

(13) Biot, C.; Buisine, E.; Rooman, M. *J. Am. Chem. Soc.* **2003**, *125*, 13988.

(14) Shi, Z.; Olson, C. A.; Kallenbach, N. R. *J. Am. Chem. Soc.* **2002**, *124*, 3284.

(15) Crowley, P. B.; Golovin, A. *Proteins: Struct., Funct., Bioinf.* **2005**, *59*, 231.

(16) Biot, C.; Wintjens, R.; Rooman, M. *J. Am. Chem. Soc.* **2004**, *126*, 6220.

(17) Wintjens, R.; Lievin, J.; Rooman, M.; Buisine, E. *J. Mol. Biol.* **2000**, *302*, 395.

(18) Gallivan, J. P.; Dougherty, D. A. *Proc. Natl. Acad. Sci. U.S.A.* **1999**, *96*, 9459.

(19) Gromiha, M. M.; Santhosh, C.; Suwa, M. *Polymer* **2004**, *45*, 633.

(20) Choi, H. S.; Suh, S. B.; Cho, S. J.; Kim, K. S. *Proc. Natl. Acad. Sci. U.S.A.* **1998**, *95*, 12094.

(21) McFail-Isom, L.; Shui, X.; Williams, L. D. *Biochemistry* **1998**, *37*, 17105.

(22) Šponer, J.; Leszczynski, J.; Hobza, P. *Biopolymers* **2002**, *61*, 3.

(23) Primet, M.; Garbowski, E.; Mathieu, M. V.; Imelik, B. *J. Chem. Soc., Faraday Trans. 1* **1980**, *76*, 1942.

(24) Hashimoto, S.; Ikuta, S.; Asahi, T.; Masuhara, H. *Langmuir* **1998**, *14*, 4284.

(25) Mentzen, B. R.; Gélin, P. *Mater. Res. Bull.* **1998**, *33*, 109.

(26) Zhu, D.; Herbert, B. E.; Schlautman, M. A.; Carraway, E. R. *J. Environ. Qual.* **2004**, *33*, 276.

(27) Goshe, A. J.; Crowley, J. D.; Bosnich, B. *Helv. Chim. Acta* **2001**, *84*, 2971.

(28) Klärner, F.-G.; Kahlert, B. *Acc. Chem. Res.* **2003**, *36*, 919.

(29) Cametti, M.; Nissinen, M.; Cort, A. D.; Mandolini, L.; Rissanen, K. *J. Am. Chem. Soc.* **2005**, *127*, 3831.

(30) Reddy, A. S.; Sastry, G. N. *J. Phys. Chem. A* **2005**, *109*, 8893.

(31) Woodin, R. L.; Beauchamp, J. L. *J. Am. Chem. Soc.* **1978**, *100*, 501.

(32) Gokel, G. W.; Barbour, L. J.; De Wall, S. L.; Meadows, E. S. *Coord. Chem. Rev.* **2001**, *222*, 127.

(33) De Wall, S. L.; Meadows, E. S.; Barbour, L. J.; Gokel, G. W. *Proc. Natl. Acad. Sci. U.S.A.* **2000**, *97*, 6271.

(34) Meadows, E. S.; De Wall, S. L.; Barbour, L. J.; Gokel, G. W. *J. Am. Chem. Soc.* **2001**, *123*, 3092.

(35) Gokel, G. W.; Barbour, L. J.; Ferdani, R.; Hu, J. *Acc. Chem. Res.* **2002**, *35*, 878.

(36) Hu, J.; Barbour, L. J.; Ferdani, R.; Gokel, G. W. *Chem. Commun.* **2002**, 1806.

(37) Hu, J.; Barbour, L. J.; Gokel, G. W. *Proc. Natl. Acad. Sci. U.S.A.* **2002**, *99*, 5121.

(38) Isupov, M. N.; Antson, A. A.; Dodson, E. J.; Dodson, G. G.; Dementieva, I. S.; Zakomirdina, L. N.; Wilson, K. S.; Dauter, Z.; Lebedev, A. A.; Harutyunyan, E. H. *J. Mol. Biol.* **1998**, *276*, 603.

(39) Frydman, L. *Annu. Rev. Phys. Chem.* **2001**, *52*, 463.

(40) Ashbrook, S. E.; Duer, M. J. *Concepts Magn. Reson.* **2006**, *28A*, 183.

(41) Power, W. P.; Wasylishen, R. E.; Mooibroek, S.; Pettitt, B. A.; Danchura, W. *J. Phys. Chem.* **1990**, *94*, 591.

(42) Chu, P. J.; Gerstein, B. C. *J. Chem. Phys.* **1989**, *91*, 2081.

(43) Matthews, S. E.; Rees, N. H.; Felix, V.; Drew, M. G. B.; Beer, P. D. *Inorg. Chem.* **2003**, *42*, 729.

(44) Lhotak, P.; Nakamura, R.; Shinkai, S. *Supramol. Chem.* **1997**, *8*, 333.

(45) Wong, A.; Whitehead, R. D.; Gan, Z.; Wu, G. *J. Phys. Chem. A* **2004**, *108*, 10551.

(46) Watts, A. *Mol. Membr. Biol.* **2002**, *19*, 267.

(47) Williamson, P. T. F.; Meier, B. H.; Watts, A. *Eur. Biophys. J.* **2004**, *33*, 247.

(48) Zhong, W.; Gallivan, J. P.; Zhang, Y.; Li, L.; Lester, H. A.; Dougherty, D. A. *Proc. Natl. Acad. Sci. U.S.A.* **1998**, *95*, 12088.

(49) Dumazy, Y.; Amoureux, J.-P.; Fernandex, C. *Mol. Phys.* **1997**, *90*, 959.

(50) Bodart, P. R.; Amoureux, J.-P.; Dumazy, Y.; Lefort, R. *Mol. Phys.* **2000**, *98*, 1545.

(51) Amoureux, J.-P.; Fernandez, C.; Steuernagel, S. *J. Magn. Reson., Ser. A* **1996**, *123*, 116.

(52) Harris, R. K.; Nesbitt, G. J. *J. Magn. Reson.* **1988**, *78*, 245.

(53) Eichele, K.; Wasylishen R. E. *WSOLIDS NMR Simulation Package*, version 1.17.30; Universitat Tuebingen: Tuebingen, Germany, 2001. See also http://casgm3.anorg.chemie.uni-tuebingen.de/klaus/soft/index.html.

(54) Massiot, D.; Fayon, F.; Capron, M.; King, I.; Le Calvé, S.; Alonso, B.; Durand, J.-O.; Bujoli, B.; Gan, Z.; Hoatson, G. *Magn. Reson. Chem.* **2002**, *40*, 70.

(55) Frisch, M. J.; Trucks, G. W.; Schlegel, H. B.; Scuseria, G. E.; Robb, M. A.; Cheeseman, J. R.; Montgomery, J. A., Jr.; Vreven, T.; Kudin, K. N.; Burant, J. C.; Millam, J. M.; Iyengar, S. S.; Tomasi, J.; Barone, V.; Mennucci, B.; Cossi, M.; Scalmani, G.; Rega, N.; Petersson, G. A.; Nakatsuji, H.; Hada, M.; Ehara, M.; Toyota, K.; Fukuda, R.; Hasegawa, J.; Ishida, M.; Nakajima, T.; Honda, Y.; Kitao, O.; Nakai, H.; Klene, M.; Li, X.; Knox, J. E.; Hratchian, H. P.; Cross, J. B.; Bakken, V.; Adamo, C.; Jaramillo, J.; Gomperts, R.; Stratmann, R. E.; Yazyev, O.; Austin, A. J.; Cammi, R.; Pomelli, C.; Ochterski, J. W.; Ayala, P. Y.; Morokuma, K.; Voth, G. A.; Salvador, P.; Dannenberg, J. J.; Zakrzewski, V. G.; Dapprich, S.; Daniels, A. D.; Strain, M. C.; Farkas, O.; Malick, D. K.; Rabuck, A. D.; Raghavachari, K.; Foresman, J. B.; Ortiz, J. V.; Cui, Q.; Baboul, A. G.; Clifford, S.; Cioslowski, J.; Stefanov, B. B.; Liu, G.; Liashenko, A.; Piskorz, P.; Komaromi, I.; Martin, R. L.; Fox, D. J.; Keith, T.; Al-Laham, M. A.; Peng, C. Y.; Nanayakkara, A.; Challacombe, M.; Gill, P. M. W.; Johnson, B.; Chen, W.; Wong, M. W.; Gonzalez, C.; Pople, J. A. *Gaussian 03*, revisions B.04 and C.02; Gaussian, Inc.: Wallingford, CT, 2004.

(56) Becke, A. D. *J. Chem. Phys.* **1993**, *98*, 5648.

(57) Pyykkö, P. *Mol. Phys.* **2001**, *99*, 1617.

(58) Dennington, R., II; Keith, T.; Millam, J.; Eppinnett, K.; Hovell, W. L.; Gilliland, R. *GaussView*, version 3.09; Semichem. Inc.: Shawnee Mission, KS, 2003.

(59) Wong, A.; Wu, G. *J. Phys. Chem. A* **2000**, *104*, 11844.

(60) Pietrass, T.; Burkert, P. K. *Magn. Reson. Chem.* **1993**, *31*, 709.

(61) Detellier, C. In *NMR of Newly Accessible Nuclei, Volume 2: Chemically and Biochemically Important Elements*; Laszlo, P., Ed.; Academic Press: New York, 1983; Chapter 5.

(62) Bisnaire, M.; Detellier, C.; Nadon, D. *Can. J. Chem.* **1982**, *60*, 3071.

(63) Willans, M. J.; Schurko, R. W. *J. Phys. Chem. B* **2003**, *107*, 5144.

(64) Samoson, A. *Chem. Phys. Lett.* **1985**, *119*, 29.

(65) Hu, J.; Barbour, L. J.; Ferdani, R.; Gokel, G. W. *Chem. Commun.* **2002**, 1810.

(66) Frydman, L.; Harwood, J. S. *J. Am. Chem. Soc.* **1995**, *117*, 5367.

(67) Medek, A.; Harwood, J. S.; Frydman, L. *J. Am. Chem. Soc.* **1995**, *117*, 12779.

(68) Medek, A.; Frydman, L. *J. Braz. Chem. Soc.* **1999**, *10*, 263.

(69) Grant, C. V.; McElheny, D.; Frydman, V.; Frydman, L. *Magn. Reson. Chem.* **2006**, *44*, 366.

(70) Mason, J. *Solid State Nucl. Magn. Reson.* **1993**, *2*, 285.

(71) Arfken, G. B. *Mathematical Methods for Physicists*; Academic Press: New York, 1985.

(72) Sagnowski, S. F.; Sułek, Z.; Stachura, M.; Ogar, J. *Z. Phys. B: Condens. Matter* **1982**, *46*, 123.

(73) Dunning, T. H., Jr. *J. Chem. Phys.* **1989**, *90*, 1007.

(74) Woon, D. E.; Dunning, T. H., Jr. *J. Chem. Phys.* **1995**, *103*, 4572.

(75) Pickard, C. J.; Mauri, F. In *Calculation of NMR and EPR Parameters. Theory and Applications*; Kaupp, M., Bühl, M., Malkin, V. G., Eds.; Wiley-VCH Verlag GmbH & co. KGaA: Weinheim, Germany, 2004; Chapter 16.

(76) Ramsey, N. F. *Molecular Beams*; Oxford University Press: London, 1956; pp 162−166, 208−213.

(77) Ramsey, N. F. *Phys. Rev.* **1950**, *77*, 567.

(78) Ramsey, N. F. *Phys. Rev.* **1950**, *78*, 699.

(79) Ramsey, N. F. *Phys. Rev.* **1951**, *83*, 540.

(80) Ramsey, N. F. *Phys. Rev.* **1952**, *86*, 243.

(81) Jameson, C. J. In *Encyclopedia of Nuclear Magnetic Resonance*; Grant, D. M., Harris, R. K., Eds.; Wiley: Chichester, U.K., 1996; p 1273.

(82) Jameson, C. J. In *Multinuclear NMR*; Mason, J., Ed.; Plenum Press: New York, 1987; Chapter 3 and references therein.

(83) Ruan, C.; Yang, Z.; Hallowita, N.; Rodgers, M. T. *J. Phys. Chem. A* **2005**, *109*, 11539.

(84) Petersen, F. N. R.; Jensen, M. Ø.; Nielsen, C. H. *Biophys. J.* **2005**, *89*, 3985.